J Mater Sci (2009) 44:84–92
DOI 10.1007/s10853-008-3067-2

Reaction of $CaAl_4O_7$ with (0001)-oriented α-Al_2O_3

A. Altay · C. B. Carter · M. A. Gülgün

Received: 2 October 2008 / Accepted: 15 October 2008 / Published online: 5 December 2008

Abstract Reactions between thin films of CA_2 and (0001)-oriented α-Al_2O_3 have been studied using a combination of microscopy techniques. Thin films of amorphous CA_2 were deposited on sapphire substrates by pulsed-laser deposition at 900 °C in an oxygen ambient atmosphere. After deposition, the reaction couples were heat treated in air for various times either at 1300 or 1400 °C. Atomic-force microscopy was used to monitor changes in the microstructure of the films. Interfaces between the different regions were examined by transmission electron microscopy (TEM) of cross-sectional samples prepared by focused ion-beam milling. The CA_2 films had dewetted the substrate surface as a result of the heat treatment. An interfacial reaction layer was observed between the dewetted CA_2 droplets and the substrate. The structure of this reaction layer was found to be consistent with γ-Al_2O_3 by computer analysis of high-resolution TEM images. There is a perfect epitaxy between the interfacial layer and the substrate. For the samples heat treated for longer times, hexagonal features were found on the substrate surface. The presence of these features on (0001)-oriented α-Al_2O_3 suggests that CA_6 platelets form by the transformation of the interfacial reaction layer. The results are discussed in relation to the crystallization behavior of the various calcium aluminate phases and the equilibrium-phase diagram of the CaO–Al_2O_3 system.

Present Address:
A. Altay
Envy, Energy & Environmental Investments, Inc.,
Ankara 06450, Turkey

Present Address:
C. B. Carter
Department of Chemical, Materials & Biomolecular Engineering, University of Connecticut, Storrs, CT 06269-3222, USA

A. Altay · C. B. Carter (✉)
Department of Chemical Engineering & Materials Science, University of Minnesota, Minneapolis, MN 55455, USA
e-mail: cbcarter@engr.uconn.edu

M. A. Gülgün
Sabanci University, FENS, Orhanli, Tuzla, 34956 Istanbul, Turkey

Introduction

Commercially, α-Al_2O_3 is one of the most widely used ceramic materials. Its strength, toughness, corrosion and wear resistance, and creep properties are closely related to the microstructure and interfacial chemistry of the polycrystalline material. During the last 60 years, extensive data have been gathered in the literature concerning the influence of various impurities on the properties and microstructure of this ceramic. For example, it is known that Si and Ca impurities can adversely affect the microstructure, fracture and high-temperature properties of α-Al_2O_3. When Si and Ca co-exist in the ceramic, they can cause abnormal grain growth and an elongated grain morphology and further degrade room-temperature fracture behavior and creep [1–5].

Since bulk α-Al_2O_3 has a very limited solubility for these and other impurities (for most impurities the solubility is limited to a few tens of ppm at typical processing temperatures), they strongly segregate to internal interfaces and surfaces. Thus, their effect is closely related to this segregation behavior and the change in chemistry, bonding and structure that they cause at these interfaces. Furthermore, it is known that together Si and Ca cause amorphous grain-boundary films or triple-point phases which influence the evolution of the morphology of the material [2, 6–8].

Bae and Baik [9] reported that there is a critical concentration for both Si and Ca that will trigger abnormal grain growth in the ceramic. When their samples were co-doped, these critical values were reported to be lower. These authors reported the critical concentration in terms of the total volume concentration which has little relevance for a surface-active impurity in a host, like α-Al_2O_3, since there is then minimal solubility for the dopant and the material is often engineered to have a fine-grain polycrystalline microstructure. The more relevant unit of concentration is the excess number of impurity atoms at the grain-boundary regions.

Altay and Gülgün [10] showed that the microstructural evolution in Ca-doped α-Al_2O_3 could be related to the excess concentration of the dopant at the grain boundaries. They manipulated the concentration of Ca at the grain boundaries by varying the total impurity content and the grain size. The reported [10] Ca-excess values were calculated assuming that all the impurity atoms would segregate to the grain boundaries; that is, the solubility of Ca in bulk α-Al_2O_3 was ignored. However, this analysis also assumed [10] that there was no precipitation or formation of a second phase at the triple junctions.

Second-phase precipitates of CA_6 composition have been observed in samples that were heavily doped with Ca [11–14]. The formation of CA_6 platelets in an α-Al_2O_3 matrix as a result of the addition of excess CaO or $CaCO_3$ has been reported previously [12–14]. The formation of CA_6-like phases in other α-Al_2O_3 systems has also been suggested, although second-phase precipitates were not observed in those studies [6, 15]. Brydson et al. [6] concluded that in their α-Al_2O_3/anorthite system there was an amorphous grain-boundary film with a nominal composition of CA_6 in the samples sintered at 1400 °C. Altay and Gülgün [11] reported the presence of CA_6 precipitates in α-Al_2O_3 samples that had been doped (with Ca only) above a certain Ca concentration. These CA_6 precipitates had an elongated morphology with the long facets of the precipitates parallel to long facets of the neighboring α-Al_2O_3 grains. In an earlier systematic study, crystallization of CA_6 films on basal α-Al_2O_3 was examined by Mallamaci et al. using TEM [16]. This study demonstrated the formation of orientation relationships between CA_6 and Al_2O_3 during crystallization of the CA_6 and implies that crystallization began at the interface, not at the surface.

The main objective of the present study was to resolve some of the fundamental questions concerning the formation of CA_6 precipitates and/or grain-boundary films in a Ca-doped polycrystalline α-Al_2O_3 matrix. Model experiments were designed to monitor the effects of Ca in α-Al_2O_3. For this purpose, thin films of various calcium aluminate phases were deposited onto single-crystal alumina substrates with a pre-selected surface orientation. The advantage of using this approach rather than polycrystalline substrates is that it allows the control of the interface orientation between the Ca-containing phase and alumina.

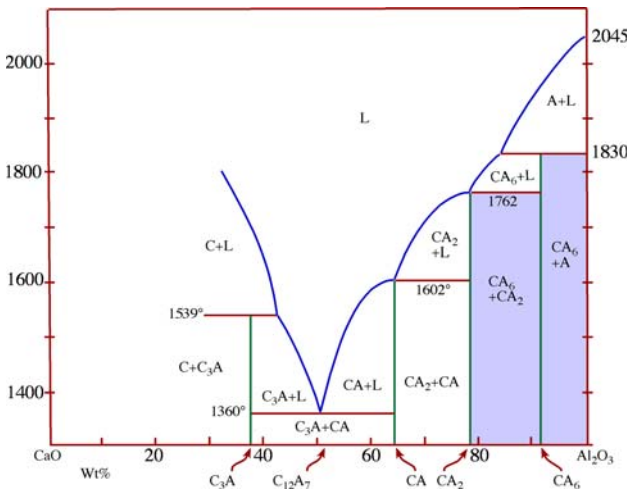

Fig. 1 Binary phase diagram of CaO–Al_2O_3 system in a moisture-free atmosphere. *C* CaO, *A* Al_2O_3 in the α form, and *L* liquid

As shown in the CaO–Al_2O_3 binary phase diagram in Fig. 1, several different calcium aluminate phases with different Ca/Al ratios can develop as the result of the high-temperature reaction between CaO and α-Al_2O_3 [17]. Among these 5 equilibrium binary compounds the two relevant to the present study, CA_2 and CA_6, have a monoclinic and a hexagonal crystal structures, respectively. Since the presence and distribution of these phases limit the performance of the refractory, their formation and interaction have been studied by several research groups [18–20]. Solid-state interactions between CaO and Al_2O_3 have been studied by Kohatsu and Brindley [18] and by Ito et al. [19]. In these studies, CaO and Al_2O_3 compacts were reacted below the lowest eutectic temperature for extended periods of time, which resulted in a layer-by-layer formation of all the calcium aluminate phases present in the phase diagram. Pt-marker experiments suggested that Ca diffused preferentially throughout the reaction layers. De Jonghe et al. [20] studied the reactions between α-Al_2O_3 and the eutectic CaO–Al_2O_3 melt at 1530 °C. In contrast to the previous studies of solid-state interactions between CaO–Al_2O_3, only the presence of a strongly textured CA_6 layer and complex phase-mixtures as additional layers were then reported [20].

In the present study, thin films of CA_2 were produced on basal α-Al_2O_3 by pulsed-laser deposition. These deposited films were heated to high temperatures, at which point they were expected to react with α-Al_2O_3 to form CA_6. Cross-sectional observations of the interfacial reactions and plane-view observations of the resulting microstructure were made as a function of temperature and time.

Experimental procedure

Samples were prepared from a (0001)-oriented α-Al_2O_3 substrate with an optically flat, polished surface (Union Carbide Corp. Crystal Products). Prior to deposition, the substrate was cut into small pieces and rinsed in a series of organic solvents, then acid cleaned and annealed at 1400 °C for 8 h. This procedure produces crystallographically flat terraces parallel to the basal plane and removes all structural surface damage [21, 22]. CA_2 powders were synthesized as the source of the film material [23]. Ceramic targets were obtained by uniaxially pressing these powders into pellets and then sintering at 1600 °C.

Pulsed-laser deposition (PLD) was used to deposit thin films of CA_2 onto the α-Al_2O_3 substrates. A KrF excimer laser (wavelength, λ, of 248 nm) was focused to a spot onto a rotating polycrystalline target to deposit CA_2 on a substrate which was maintained at a temperature of 900 °C. A pulse repetition rate of 10 Hz was used with an average energy per pulse of 100 mJ. The thickness of the film was controlled by varying the number of laser pulses: 40,000 pulses produced a CA_2 layer ~80 nm thick. All the depositions were performed in an oxygen ambient atmosphere of 20 mTorr.

The reaction couples were heat treated in air at either 1300 or 1400 °C for various times following the depositions. In order to protect the samples from Si contamination in the furnace, they were first placed in a Pt crucible. The Pt crucibles were then placed between two layers of covered α-Al_2O_3 crucibles filled with high-purity α-Al_2O_3 powders. The phase formation and the crystallinity of the films were characterized by X-ray microdiffraction (Bruker AXS). Atomic-force microscopy (AFM, DI Nanoscope III) and scanning electron microscopy (SEM, Hitachi S900 FEG) were used to monitor the microstructural changes of the films. Cross-sectional transmission electron microscope (TEM) samples were prepared by focused ion-beam (FIB, FEI Strata DB 235) milling using the self-supporting sample geometry [24]. The interfaces between the films and the substrates were examined by TEM (FEI Tecnai G2 F30 FEG and T12 LaB_6). The reaction layer between the film and the substrate was identified by Fourier analysis of the high-resolution images.

Results

Chemistry

Phase formation, crystallinity and the chemistry of the samples were determined before and after the depositions. XRD analyses that were carried out prior to the depositions confirmed that the CA_2 powders used for the target preparation were single phase and crystalline (Fig. 2a). Microdiffraction analysis showed that the CA_2 films were amorphous after the deposition and electron-probe microanalysis (Jeol 8900) confirmed that the films were stoichiometric CA_2. For the microdiffraction analysis, CA_2 films were deposited on graphite substrates under the same conditions in order to avoid the effect of the substrate composition on the chemical analysis. Measurements were taken from five different points on the film in order to check the homogeneity of the composition. Anorthite was used as the standard for the quantitative analysis. As can be seen in Table 1, the film was homogeneous with the chemistry of CA_2; however, it was contaminated with 0.4 wt% of Si at some stage before the analysis.

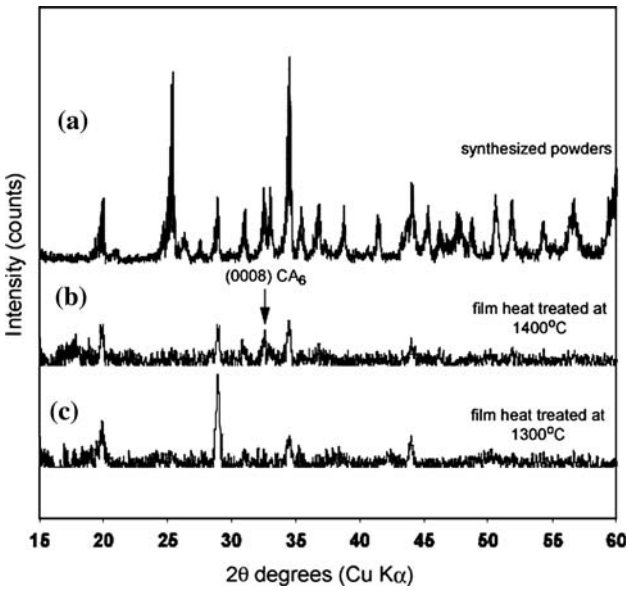

Fig. 2 XRD 2θ scans of (a) CA_2 powders synthesized by using PVA precursors, (b) CA_2 film heat treated at 1400 °C, and (c) CA_2 film heat treated at 1300 °C

These amorphous thin films on Al_2O_3 substrates were crystallized ex situ (in air) either at 1300 or 1400 °C. The crystallinity of the films was characterized by X-ray microdiffraction on the samples heat treated for 1 h at both temperatures. Figure 2b and c shows that single-phase CA_2

Table 1 Electron probe microanalysis of the CA_2 film deposited on a carbon substrate

Point #	SiO_2 (wt%)	CaO (wt%)	Al_2O_3 (wt%)	Total
1	0.4	19.7	79.9	100.0
2	0.4	19.9	79.7	100.0
3	0.4	19.5	80.1	100.0
4	0.4	19.2	80.4	100.0
5	0.4	19.8	79.8	100.0
Average	0.4	19.4	80.2	100.0

films were obtained at 1300 °C and that the CA_6 phase started to form at 1400 °C.

AFM observations

A series of height-mode AFM images shows the microstructure of the CA_2 films after the various heat treatments (Figs. 3 and 4). Figure 3a is an image of a film that has been heat treated at 1300 °C for 1 h. The film has a grainy microstructure and has started to dewet the substrate surface. Figure 3b and c shows the microstructure of a CA_2 film after the heat treatment at 1300 °C for 4 h. The variations in the film morphology can be seen on these two images taken from the same sample. While the region in Fig. 3b consists of small grains covering most of the substrate surface, the region in Fig. 3c consists of dewet droplets and an area where six-sided platelets stack on top of each other. The section analysis in Fig. 3d shows the height variations across this area.

As can be seen in Fig. 4a, the grains started to become elongated when the CA_2 film was heat treated at 1400 °C for as little as 5 min. Dewetting of the film is then well pronounced for the samples heat treated at 1400 °C for 1 h and for 4 h (Fig. 4b–d). Figure 4c and d shows two different regions on the same sample heat treated at 1400 °C for 4 h. The higher magnification image in Fig. 4d clearly shows the formation of the hexagonal crystals.

In addition to the isolated regions of six-sided crystals that are observed on the samples heat treated for 4 h, another layer of facetted crystals can be seen on the samples heat treated at both temperatures for shorter periods (Fig. 5a, b). Layers of these facetted crystals were observed on the surface where the CA_2 film dewetted. The angles between the facets are 60 and 120° as shown in Fig. 5b.

TEM observations

Montages of the cross-sectional TEM images of the CA_2 films heat treated at 1300 and 1400 °C for 1 h are shown in Fig. 6a and b, respectively. The TEM membrane that was cut from the sample heat treated at 1300 °C shows a continuous film of CA_2 with small grains. The membrane that was cut from the sample heat treated at 1400 °C contains dewet droplets of CA_2 on the α-Al_2O_3 substrate. The droplet that was analyzed by high-resolution TEM (HRTEM) is labeled as X in Fig. 6b.

An interfacial reaction occurred between the film and the substrate at both heat treatment temperatures. Figure 7a shows the interface between the droplet X and the α-Al_2O_3 substrate. This image was recorded with the electron beam

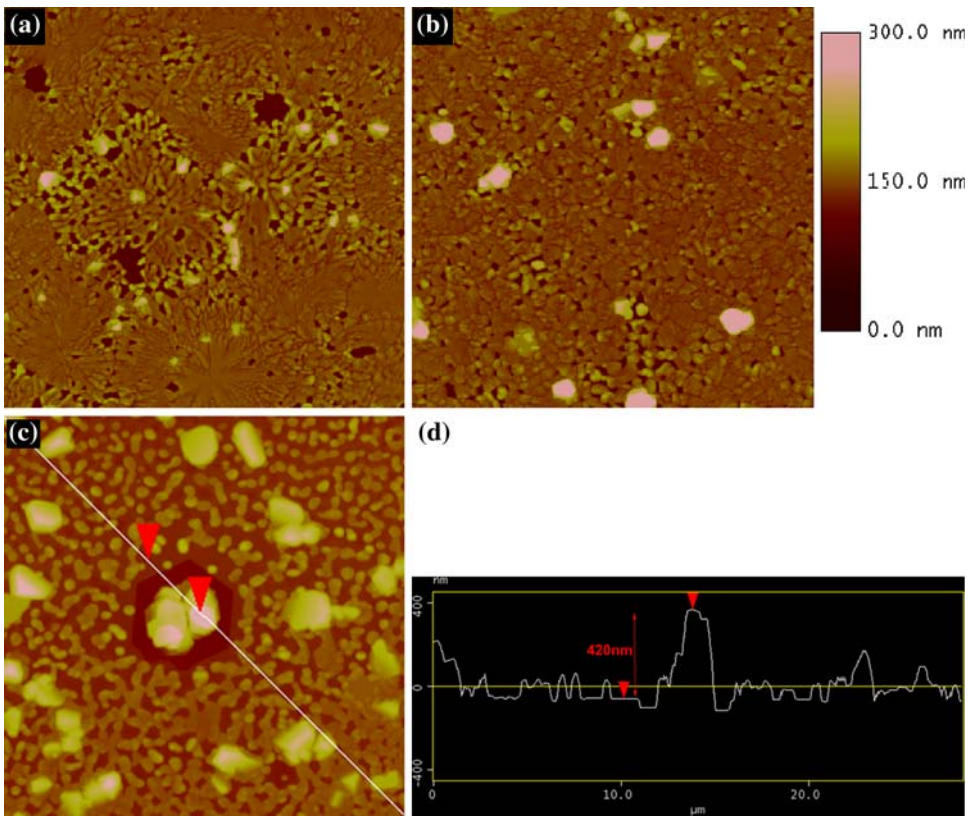

Fig. 3 Height-mode AFM images of films heat treated at **a** 1300 °C for 1 h, **b** 1300 °C for 4 h. The scans are 20 × 20 μm. **c** Height-mode AFM images of films heat treated at 1300 °C for 4 h and **d** the corresponding section analysis. The scanned area in each case is 20 × 20 μm

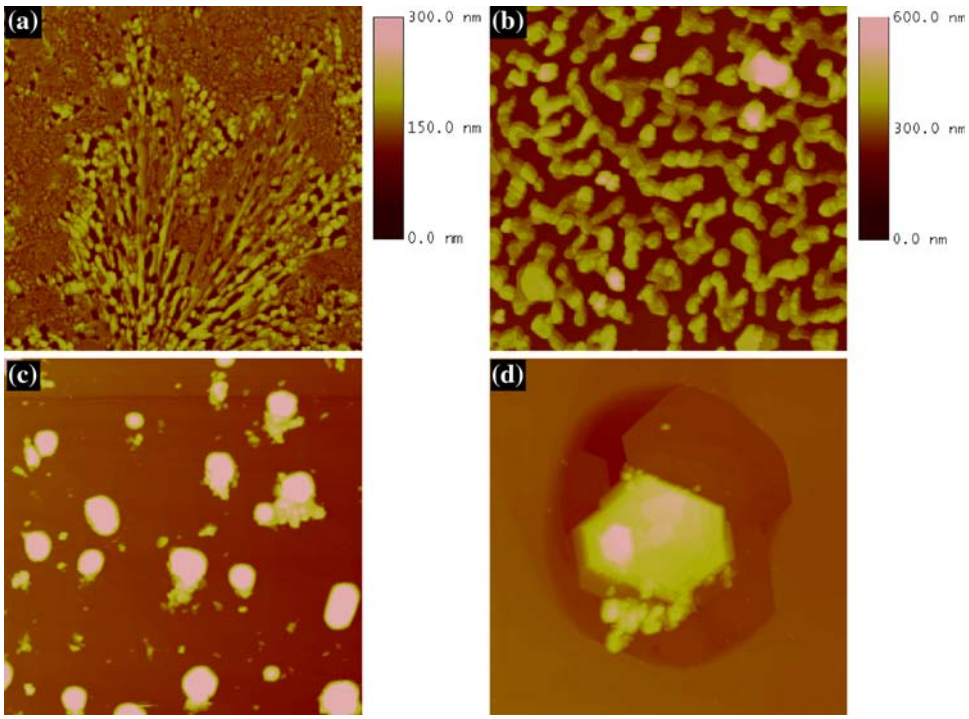

Fig. 4 Height-mode AFM images of films heat treated at **a** 1400 °C for 5 min, **b** 1400 °C for 1 h. The scans are 20 × 20 μm. **c**, **d** Height-mode AFM images of the films heat treated at 1400 °C for 4 h. **c** 20 × 20 μm and **d** 7 × 7 μm

parallel to the $[2\bar{1}\bar{1}0]$ zone axis of the α-Al_2O_3 substrate. Since it was not possible to obtain a selected-area diffraction pattern (SADP) solely from the 5-nm-thick reaction layer, Fourier analysis of the image was used to identify the phase at the interface (Fig. 7b). From the analysis of the *d*-spacings and the angles between the systematic rows of reflections observed in the (fast) Fourier transform (FFT) of the image, the reaction layer at the interface is identified as γ-Al_2O_3. An epitactic relationship was observed between the reaction layer and the substrate. As illustrated by the schematic of the FFT in Fig. 8 taken from the interfacial region, this epitactic relationship was $(111)_\gamma \| (0001)_\alpha$ and $[112] \| [2\bar{1}\bar{1}0]$. A similar reaction layer at the interface with the same epitactic relationship was also observed on the sample heat treated at 1300 °C.

The schematic of the SADP in Fig. 9 shows the orientation relationship between the CA_2 droplet (droplet X) and the α-Al_2O_3 substrate that was obtained from the HRTEM image in Fig. 7a. Although the film and the substrate were oriented with the [107] and $[2\bar{1}\bar{1}0]$ zone axes parallel, no additional orientation relationship between this droplet and the substrate is apparent.

Discussion

The afore-mentioned results give two types of information, namely what phases form and why these phases form even though they are not exactly as expected from the equilibrium phase diagram.

Formation of new phases: γ-Al_2O_3 and CA_6

The thin films of CA_2 were amorphous in their as-deposited state and crystallized during the post-deposition heat treatments at 1300 and 1400 °C. During these heat treatments the films also reacted with the α-Al_2O_3 substrates. Although these temperatures are lower than the melting point of CA_2, they were specifically chosen since 1300 °C is slightly below and 1400 °C is slightly above the first eutectic temperature in the CaO–Al_2O_3 binary system [17]. It had been previously proposed that pre-melting can occur at the interfaces due to the preferential alignment or segregation of cations [25, 26]. If a melt formed at the interface during the reaction between the CA_2 film and the alumina substrate, then the effect should be seen after heat-treatment at a temperature slightly above the first eutectic temperature. A comparison of the experimental observations on the samples heat treated at 1300 and 1400 °C, however, did not show any evidence of melting at the interface.

According to the phase diagram in Fig. 1, it is expected that CA_6 will form by the reaction between the CA_2 and α-Al_2O_3 in the solid state, or from the liquid phase if the temperature is high enough [18–20]. However, the formation of γ-Al_2O_3 prior to the formation of CA_6 has not been reported in previous studies [18–20]. There may be several reasons why the formation of γ-Al_2O_3 was not previously observed. For example, the instruments that were available when the earlier studies were conducted might not have had sufficient resolution to observe the interface structures

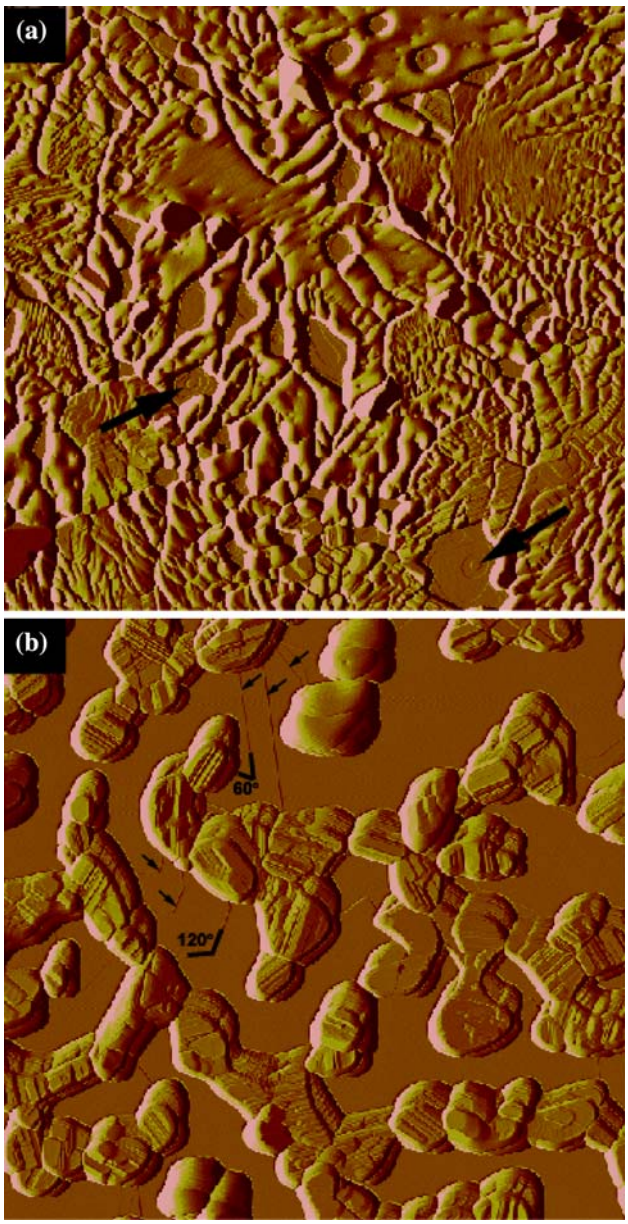

Fig. 5 Deflection-mode AFM images of films heat treated at **a** 1300 °C for 1 h and **b** 1400 °C for 1 h. Facetted regions on the surface identified by *arrows*. Scanned areas are 10 × 10 μm

Fig. 6 Montages of the cross-sectional TEM images of films heat treated at **a** 1300 °C for 1 h, **b** 1400 °C for 1 h. The *dark layer* is the Pt coating used to protect the original surface during FIB preparation

at the atomic scale or the reaction temperatures might be too high. Furthermore, the duration of the reaction at these temperatures might easily be too long so that a metastable phase such as γ-Al_2O_3 would have already transformed. In addition to the reactions between the calcium aluminate phases, the synthesis and crystallization of these phases have also been studied extensively [27–31]. In some of these studies, it was reported that calcium aluminate powders which contain up to 25 mol% of CaO crystallize by first forming a γ-Al_2O_3 solid solution [27–30]. The details of the crystallization of the CA_2 and CA_6 powders have now been reported [23] and discussed in comparison to the previous studies in the literature. In this recent study [23], the formation of γ-Al_2O_3-Ca solid solution was also confirmed unambiguously using the TEM and by ELNES analysis.

In the present study, a different approach was used to examine the formation of CA_6 in addition to the crystallization. Thin films of amorphous CA_2 were prepared by laser deposition in a high-vacuum chamber under 20 mTorr O_2 atmosphere and reacted with the α-Al_2O_3 substrates at 1300 and 1400 °C. Therefore, stabilization of γ-Al_2O_3 by the presence of adsorbed H_2O is not a likely contributing factor. Previously, the highest temperature at which γ-Al_2O_3 has been observed was 1160 °C [30]. However, γ-Al_2O_3 was found in the samples heat treated at 1300 and 1400 °C for 1 h in this study. The stability of metastable phases has been studied and discussed for several systems [32, 33]. The growth of metastable phases on substrates that provide a suitable template for the non-equilibrium phase has been reported [32, 33]. It is thus proposed that γ-Al_2O_3 can be stabilized at temperatures as high as 1400 °C when it is spatially confined at the interface between the CA_2 and α-Al_2O_3. The possibility that the γ-Al_2O_3 layer is formed during cooling would require significant solid-state diffusion of Ca out of this layer and is not likely to occur.

As noted previously, CA_6 should form by the reaction between the CA_2 film and the alumina substrate [18]. Although the presence of CA_6 was not observed in the TEM samples, the microdiffraction results do show the presence of the CA_6 phase in the sample heat treated at 1400 °C. The TEM specimens are, of course, only representative of a 20-μm region of the reaction couples. It was shown by Mallamaci et al. that the relationship between the (0001)-oriented α-Al_2O_3 and CA_6 is $(0001)_{CA_6}\|(0001)_{\alpha\text{-}Al_2O_3}$, which is in agreement with the microdiffraction results obtained in the present study. CA_6 consists of layers of spinel blocks $(Al_{11}O_{16})^+$ separated by mirror planes in which Ca^{2+} cations reside [34]. The cubic packing of the O and Al atoms of the spinel blocks found in CA_6 are similar to that found in γ-Al_2O_3, with the orientation relationship of $(0001)_{CA_6}\|(111)_{\gamma\text{-}Al_2O_3}$ [29]. These orientation relationships are consistent with the epitactic relationship found here between γ-Al_2O_3 and α-Al_2O_3 i.e., $(111)_\gamma\|(0001)_\alpha$. The presence of perfectly aligned γ-Al_2O_3

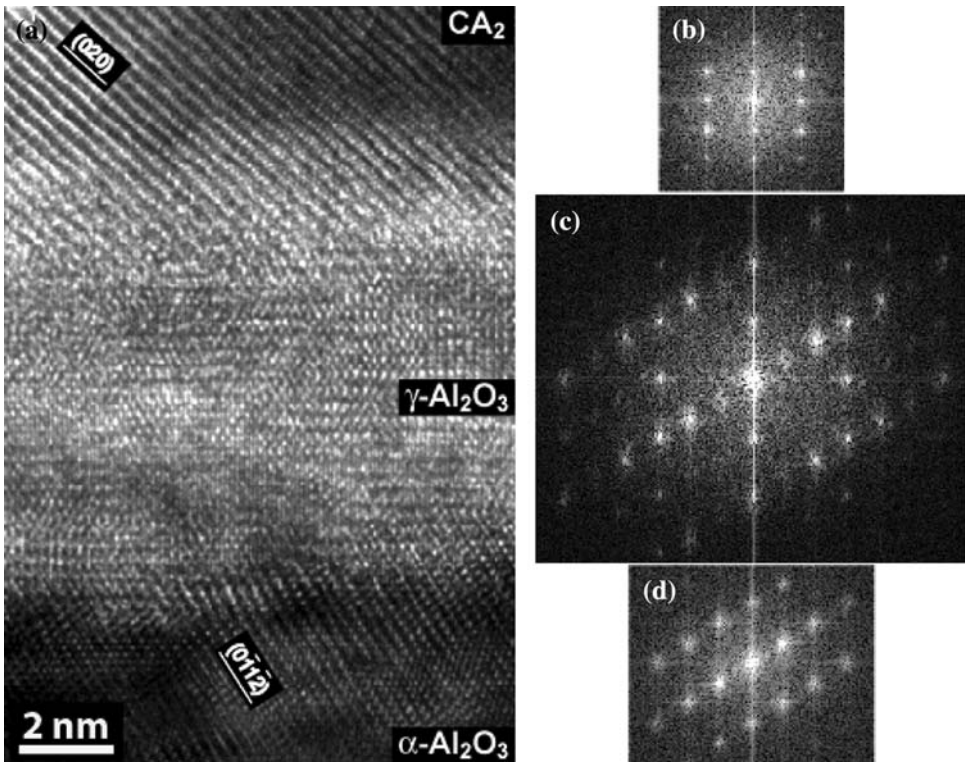

Fig. 7 **a** HRTEM image of the film heat treated at 1400 °C for 1 h. The crystallography of the three regions is determined from the FFTs in (**b**–**d**); FFT of **b** the reaction layer, **c** the substrate, and **d** the interface between the reaction layer and the substrate shown in (**a**)

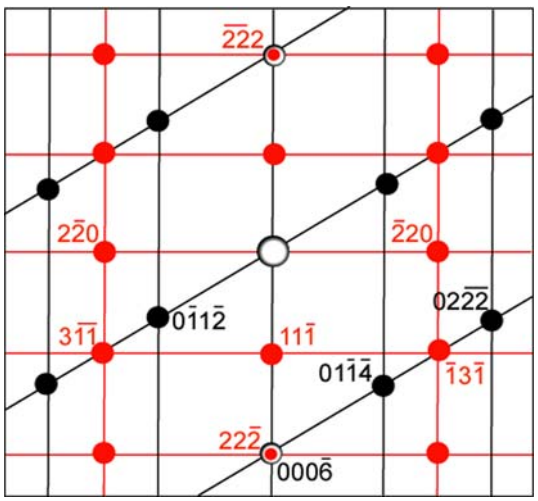

Fig. 8 Schematic of the FFT of the interface between the reaction layer and the substrate shown in Fig. 7a. *Red spots* and *lines* represent γ-Al_2O_3; *black spots* and *lines* represent α-Al_2O_3. The zone axis is [112] for γ-Al_2O_3 and [2$\bar{1}\bar{1}$0] for α-Al_2O_3

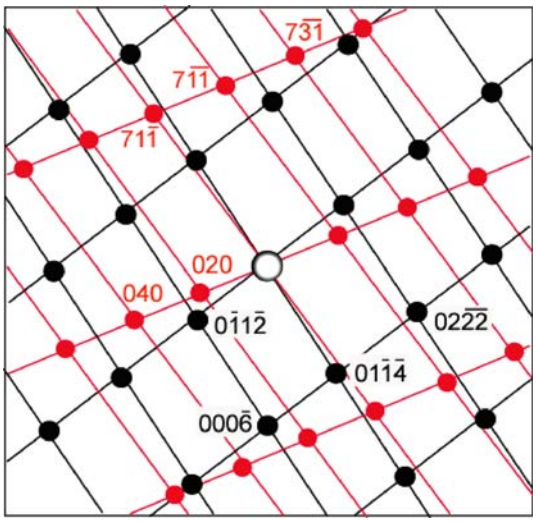

Fig. 9 Schematic of the SAD pattern of the interface between the CA_2 film and the substrate shown in Fig. 7a. *Red spots* and *lines* represent CA_2; *black spots* and *lines* represent α-Al_2O_3. The zone axis is [107] for CA_2 and [2$\bar{1}\bar{1}$0] for α Al_2O_3

should allow the easier formation of CA_6 if the growth occurs with the Al_2O_3 building blocks. Previously, Morrissey et al. [35] observed a similar behavior for the growth of β'''-Al_2O_3 second-phase particles into spinel second-phase particles that were present in a commercial α-Al_2O_3: the longer axes of the β'''-Al_2O_3 particles were always parallel to the basal plane of the α-Al_2O_3 and a {111} plane of the spinel [35]. β'''-Al_2O_3 also consists of layers of spinel blocks similar to CA_6 and the orientation relationship observed between the β'''-Al_2O_3 second-phase particles and spinel second-phase particles agrees with the orientation relationship between CA_6 and γ-Al_2O_3. A related orientation relationship was found for β-alumina growing directly into α-Al_2O_3 [36].

When the duration of the heat treatment at either temperature was increased from 1 to 4 h, evidence for the

presence of CA_6 was also found in the AFM images. As seen in the Figs. 3c and 4d, six-sided platelets have formed on the surface. The shape of these platelets indicates that they are parallel to the common (0001) planes as suggested with the orientation relationship between CA_6 and α-Al_2O_3. Therefore, it is proposed that by increasing the duration of the heat treatment even at 1300 °C, sufficient time is then available for the Ca^{2+} diffusion to produce significant amounts of CA_6. As shown in Fig. 5b, the angles between the facets of the layers on the surface also reflect the hexagonal symmetry of the CA_6 phase.

Dewetting of the thin film of CA_2

The cross-sectional images in Fig. 6 and their analysis in Figs. 7 and 8 show that the continuous film dewets the surface but it may leave a very thin wetting layer in contact with the α-Al_2O_3 (essentially a Stranski–Krastanow mechanism).

Another important observation in this study is the dewetting of the CA_2 films on the α-Al_2O_3 surface. Since there is no evidence of melting, it is suggested that dewetting occurred in the solid state as was previously observed for anorthite on sapphire [37].

As the amorphous CA_2 films crystallize during the heat treatments, the volume of the film decreases due to densification. Therefore, depending on the total density change during crystallization the films can dewet (or uncover) the surface. If this mechanism occurred in the present study, then once the films were fully crystallized, dewetting should have stopped and the microstructure on the surface should have been similar for the samples heat treated at 1300 and 1400 °C. As shown in Figs. 3 and 4, the dewetting behavior of the film changed as the temperature and duration of the heat-treatment were changed. Thin films on a substrate form islands on continued heating if the interfacial energy is not very small [37, 38]. The instability of polycrystalline thin films has been calculated theoretically and examined experimentally for ZrO_2 thin films [38]. In that case it was reported that when the ratio of grain size to film thickness exceeds a critical value, the film breaks up to lower the total free energy of the system. Similarly, crystalline anorthite films converted to arrays of islands when the films were annealed at 1200 °C [37]. Other than the ceramic thin films, such behavior has been observed for a variety of metal films including Ni [39], Au [39–42], Ag [43, 44], Sn [45, 46], Cu [47] and Pt [48]. In these studies, holes were formed on the film and then grew and coalesced. It should be noted that similar results have been described in the literature using different terminologies: the solid-state process has been described as "solid-state dewetting" or "de-sintering" or more descriptively by "the film uncovers the surface" or "the film breaks up into islands".

In the present study, the polycrystalline CA_2 films were formed after crystallization and they dewetted the surface as the temperature and duration of the heat treatments were increased. This dewetting behavior might be related to a critical grain size to film thickness ratio [38]. However, in this study the CA_2 grains did not only grow, they also reacted with the substrate. The importance of compound formation in reactive wetting for metal/ceramic systems has been widely investigated [49–51]. Although those studies showed that the spreading kinetics was strongly influenced by the formation of a compound at the interface, they only considered the reaction between a liquid metal drop and a smooth ceramic surface. Parameters such as fluid flow were included in the calculations [49–51] which cannot be used if the reaction and spreading occur in the solid state. A full description of the dewetting of CA_2 on Al_2O_3 requires further analysis; it cannot be explained only by considering the ratio of critical grain size to film thickness or by an extension of the reactive-wetting kinetics derived for metal/ceramic systems.

Conclusions

Calcium is a common impurity in commercial α-Al_2O_3. Calcium atoms segregate to grain boundaries and form CA_6 second-phase precipitates. In order to investigate the formation of the CA_6 precipitates, thin films of amorphous CA_2 were deposited onto single-crystal α-Al_2O_3 substrates with selected surface orientation. This study also allowed examination of the structure of the interface between the Ca-containing phase and α-Al_2O_3 while the reaction occurred. Although CA_6 can crystallize when in contact with (0001) α-Al_2O_3, the structure of the CA_2 is very different and the interfaces are thus very different; both the CA_2/CA_6 and the CA_2/α-Al_2O_3 interfaces are expected to have high energies. Ultimately, it is expected that the layer will transform to CA_6 and again wet the α-Al_2O_3.

The CA_2 films crystallized and dewetted the surface during the post-deposition heat treatments. The reaction product formed between the film and the substrate during these heat treatments was identified by HRTEM to be γ-Al_2O_3. The presence of γ-Al_2O_3 in the samples heat treated at 1300 and 1400 °C was not initially expected; the stabilization of this phase at the temperatures as high as 1400 °C is proposed to be an effect of the interface. Previous reports suggesting that γ-Al_2O_3 can incorporate Ca have been confirmed directly; the present report emphasizes the crystallographic relationships between γ-Al_2O_3, CA_6 and α-Al_2O_3. It is proposed that the formation of CA_6 in α-Al_2O_3 can be preceded by the transformation of the γ-Al_2O_3-Ca solid solution. The mechanism by which solid-state dewetting of the CA_2 film takes place is still not known.

Acknowledgements The work was initially supported by U.S. Department of Energy through grant DE-FG02-01ER45883 and subsequently by the 3M Harry Heltzer Endowed Chair, an NSF international travel grant INT-0322622 and a Turkish Science and Technology Foundation TUBITAK Bilateral Travel grant 103M038. The authors thank Dr. U. Dahmen for access to the FIB at the National Center for Electron Microscopy, Lawrence Berkeley National Laboratory; NCEM is supported by the U.S. Department of Energy under Contract # DE-AC02-05CH11231.

References

1. Hansen SC, Philips DS (1983) Philos Mag 47:209
2. Bae IJ, Baik S (1996) Mater Sci Forum 204–206:485
3. Bae IJ, Baik S (1997) J Am Ceram Soc 80:1149
4. Cook RF, Schrott AG (1988) J Am Ceram Soc 71:50
5. Handwerker CA, Morris PA, Coble RL (1989) J Am Ceram Soc 72:130
6. Brydson R, Chen SC, Riley FL, Milne SJ (1998) J Am Ceram Soc 81:369
7. Park SY (1996) J Mater Sci Lett 15:878
8. Ravishankar N, Carter CB (2001) Acta Mater 49:1963
9. Bae SI, Baik S (1993) J Am Ceram Soc 76:1065
10. Altay A, Gülgün MA (2003) J Am Ceram Soc 86:623
11. Altay A, Gülgün MA (2004) Key Eng Mater 264–268:219
12. Belmonte M, Sanchezherencia AJ, Moreno R, Miranzo P, Moya JS, Tomsia AP (1993) J Phys IV 3:1443
13. Nagaoka T, Yasuoka M, Hirao K, Kanzaki S, Yamaoka Y (1996) J Mater Sci Lett 15:1815
14. Powell-Dogan CA, Heuer AH (1990) J Am Ceram Soc 73:3670
15. Kaplan WD, Mullejans H, Ruhle M (1995) J Am Ceram Soc 78:2841
16. Mallamaci MP, Sartain KB, Carter CB (1998) Philos Mag A 77:561
17. Nurse RW, Welch JH, Majumdar AJ (1965) Br Ceram Trans 64:409
18. Kohatsu I, Brindley GW (1968) Z Phys Chem Neue Folge 60:79
19. Ito S, Kato M, Suzuki K, Inagaki M (1977) Z Phys Chem Neue Folge 104:147
20. De Jonghe LC, Schmid H, Chang M (1984) J Am Ceram Soc 67:27
21. Norton MG, Summerfelt SR, Carter CB (1990) Appl Phys Lett 56:2246
22. Susnitzky DW, Carter CB (1992) J Am Ceram Soc 75:2463
23. Altay A (2006) Calcium aluminate in alumina. PhD thesis, University of Minnesota
24. Perrey CR, Carter CB, Michael JR, Kotula PG, Stach EA, Radmilovic VR (2004) J Microsc 214:222
25. Zhang S, Garofalini SH (2005) J Am Ceram Soc 88:202
26. Su X, Garofalini SH (2005) J Appl Chem 97:113526
27. Vallino M (1984) Ceram Int 10:30
28. Douy A, Gervais M (2000) J Am Ceram Soc 83:70
29. Cinibulk MK (1998) J Am Ceram Soc 81:3157
30. MacKenzie KJD, Schmucker M, Smith ME, Poplett IJF, Kemmitt T (2000) Thermochim Acta 363:181
31. Tas AC (1998) J Am Ceram Soc 81:2853
32. Prinz GA (1985) Phys Rev Lett 54:1051
33. Herr U (2000) Contemp Phys 41:93
34. Utsunomiya A, Tanaka K, Morikawa H, Marumo F, Kojima H (1988) J Solid State Chem 75:197
35. Morrissey KJ, Carter CB (1983) In: Rossington DR, Condrate RA, Snyder RL (eds) Advances in materials characterization, vol 15. Plenum Press, Alfred, NY, p 297
36. Susnitzky DW, Carter CB (1986) J Am Ceram Soc 69:C25
37. Mallamaci MP, Carter CB (1999) J Am Ceram Soc 82:33
38. Miller KT, Lange FF, Marshall DB (1990) J Mater Res 5:151
39. Gimpl ML, McMaster AD, Fuschillo N (1964) J Appl Phys 35:3572
40. Kane WM, Spratt JP, Hershinger LW (1966) J Appl Phys 37:2085
41. Hummel RE, DeHoff RT, Matts-Goho S, Goho WM (1981) Thin Solid Films 78:1
42. Lee SY, Hummel RE, Dehoff RT (1987) Thin Solid Films 149:29
43. Sharma SK, Spitz J (1980) Thin Solid Films 66:51
44. Sharma SK, Spitz J (1980) Thin Solid Films 67:109
45. Caswell HL, Budo Y (1964) J Appl Phys 35:644
46. Scharnhorst P (1969) Surf Sci 15:380
47. Bachmann L, Sawyer DL, Siegel BM (1965) J Appl Phys 36:304
48. Wu NL, Phillips J (1986) J Appl Phys 59:769
49. Eustathopoulos N (1998) Acta Mater 46:2319
50. Rado C, Drevet B, Eustathopoulos N (2000) Acta Mater 48:4483
51. Saiz E, Cannon RM, Tomsia AP (2000) Acta Mater 48:4449